SI Appendix for "Growth, metabolic partitioning, and the size of microorganisms"

Christopher P. Kempes, Stephanie Dutkiewicz, Michael J. Follows

Overview This supplement contains mathematical derivations and data analyses which are outside of the scope of the main text. At the end of this supplement we provide all of the single cell growth trajectories analyzed in the main text. The data compiled for populations of organisms, which we used for interspecific analyses, is attached as a summary document (Dataset S1) and also as a digital data file (Dataset S2).

Metabolic partitioning, bioenergetic constants, and chemostat measurements In the main text we compared the energetics of a populations of cells with the parameter values that we obtained from fits of single-cell growth trajectories. Analyses of populations rests on the Pirt model [3] which linearly relates the consumption rate Q of a limiting resource to the specific growth rate μ of a population along with its yield coefficient Y and maintenance metabolism P:

$$Q = \frac{\mu}{Y} + P. \tag{S1}$$

Although the consumption rates measured in chemostat experiments may range from glucose to oxygen to light absorption it is always possible to represent this relationship in the normalized units of percentage growth and maintenance

$$1 = \frac{\mu}{Y}\frac{1}{Q} + \frac{P}{Q} \tag{S2}$$

where this equation can be compared to the single cell analysis as represented by equation 5 of the main text and discussed below. Equations 3 and 4 from the main text detail the correspondence between the Pirt population model and the single cell framework. This allows us to interpret population based values as the averages of single cell values and in particular we note that

$$\bar{E}_m = \frac{N}{Y} \tag{S3}$$

$$\bar{B}_m = PN \tag{S4}$$

and thus

$$\bar{b} \equiv \frac{B_m}{E_m} = PY \tag{S5}$$

Species	Evolutionary Life-history Grouping	Chemostat Temperature	Y	P	b		notes	Refs.
					Raw Value	Normalized to 20 ° C		
B. subtilis	Prokaryote	37 ° C	87.57 (dry g cells · mol glucose^{-1})	1.22×10^{-7} (mol glucose · s^{-1} · dry g cells^{-1})	1.07×10^{-5} (s^{-1})	2.90×10^{-6} (s^{-1})	we used the wild type values for growth on glucose	[32]
E. coli	Prokaryote	30 ° C	59.7 (dry g cells · mol O_2^{-1})	1.22×10^{-7} (mol O_2 · s^{-1} · dry g cells^{-1})	7.30×10^{-6} (s^{-1})	3.33×10^{-6} (s^{-1})	we used the glucose experiment to compare well with the growth trajectories of refs. [27, 28]	[4]
C. albicans	Eukaryote	30 ° C	.40 (dry g cells · g maltose^{-1})	4.23×10^{-6} (g maltose · s^{-1} · dry g cells^{-1})	1.68×10^{-6} (s^{-1})	7.66×10^{-7} (s^{-1})	we used the measurements for growth on maltose to be most comparable to ref.[29]	[5]
T. weissflogii	Eukaryote	18 ° C	16.70 (dry g cells · mol O_2^{-1})	2.37×10^{-8} (mol O_2 · s^{-1} · dry g cells^{-1})	3.97×10^{-7} (s^{-1})	4.67×10^{-7} (s^{-1})	estimated from the reported gross photosynthesis	[18]
Brachionus calyciflorus	Metazoan	25 ° C	—	—	3.61×10^{-6} (s^{-1})	2.43×10^{-6} (s^{-1})	measurements are given in specific ingestion rates so the units of Y and P are unclear but b can still be calculated	[19]

Table S1: Chemostat growth energetics for various organisms spanning three major evolutionary life-history transitions. The units of consumption rate Q are the same as the maintenance term P.

independent of the type of consumption being measured by Q. Here the bar notation denotes average values over a population of cells.

Thus we can calculate b from information obtained from population experiments. We first located those experiments that correspond to each of the individual species analyzed in this paper. The resulting b values are useful for informing the initial conditions of the single cell growth trajectory fits (see below), and for subsequent comparison with the best fit value of b for each trajectory. For four species (*E. coli*, *B. subtilis*, *C. albicans*, and *T. weissflogii*) we are able to directly compare our single cell analysis to chemostat experiments. For the diatom *Lauderia borealis* (eukaryotic autotroph) we used the value from *T. weissflogii* for comparison, and for *Calanus pacificus* and *Pseudocalanus sp.*, two species of copepods (multicellular heterotrophs), we used chemostat results from the rotifer *Brachionus calyciflorus*. Table S1 reports Y, and P along with the calculated value of b for each experiment along with notes on each of the sub-experiments that we used.

Compilation of b estimates from diverse species In general, a large number of experiments exist where it is possible to calculate b for a wide variety of species, and we have created a general compilation of b values from a survey of the literature (this compilation is attached as a supplementary data file and also as a PDF). Fig. S1 gives the distribution of b values for both prokaryotes and eukaryotes. For both groups the b values are approximately log-normally distributed and have means that are indistinguishable from one another ($b = 5.79 \pm 9.99 \times 10^{-6}$ for prokaryotes and $b = 3.39 \pm 3.17 \times 10^{-6}$ for eukaryotes). We were able to pair many of the compiled b estimates with measurements of cell size and estimates of body mass. These are the data presented in figure 3D of the main text. Here we find that there is no obvious relationship between b and body mass for both prokaryotes and eukaryotes.

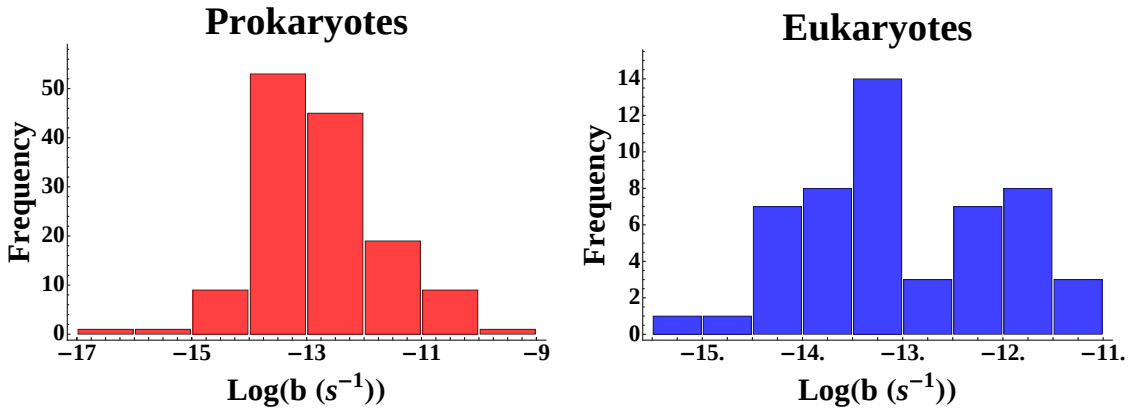

Figure S1: The distribution of b values normalized to 20° C for prokaryotes and eukaryotes. The median value for prokaryotes is $b = 2.42 \times 10^{-6}$ s^{-1} and for eukaryotes it is $b = 1.84 \times 10^{-6}$ s^{-1}. The mean value for prokaryotes is $b = 5.79 \pm 9.99 \times 10^{-6}$ which is indistinguishable from the eukaryotic value of $b = 3.39 \pm 3.17 \times 10^{-6}$.

In compiling experiments for estimating b we included a diverse set of growth conditions in order to cover a large number of species and body sizes. These conditions include growth on a range of substrates, in different experimental setups (chemostats, batch culture time evolutions, and recycling fermenters), and at various temperatures. These conditions contribute to the relatively large spread in the value of b. Some of the growth condition deviations can be systematically eliminated, using, for example, temperature normalization (see below), while others, such as growth on different substrates or in different culture setups, are more complicated to standardize. For example taking only chemostat experiments the prokaryotic mean becomes $b = 4.23 \pm 5.12 \times 10^{-6}$, which is similar to the value listed above but with much less variance. Similarly, growth on different substrates contributes to the variation in b where, for *E. coli*, ref. [4] uses the same experimental setup but alters the growth medium (Table S2) resulting in a value of b which ranges over a factor of about 2.

Substrate	Y (dry g cells $\cdot$ mol O_2^{-1})	P (mol $O_2 \cdot s^{-1} \cdot$ dry g cells^{-1})	b (s^{-1}) (Normalized to 20 $^\circ$ C)
Acetate	20.3	3.33×10^{-7}	3.09×10^{-6}
Pyruvate	34.3	2.03×10^{-7}	3.18×10^{-6}
Lactate	35	2.03×10^{-7}	3.24×10^{-6}
Glucose	59.7	1.22×10^{-7}	3.33×10^{-6}
Glycerol	50.9	1.61×10^{-7}	3.75×10^{-6}
Arabinose	57.8	1.78×10^{-7}	4.69×10^{-6}
Fructose	56	1.97×10^{-7}	5.05×10^{-6}
Fumerate	40.4	3.14×10^{-7}	5.79×10^{-6}
Galactose	58.2	2.69×10^{-7}	7.16×10^{-6}

Table S2: *E. coli* chemostat growth energetics for different substrates. All data is from Ref. [4].

Many of the studies that we compiled do not report an estimate of Y and P and in such cases we fit a linear relationship to digitized data of Q vs. μ. For multiple studies we fit only the early portion of the data (slow growth rates) where there is a clear linear relationship between Q and μ and the data agree with equation 1 of the main text. At high growth rates nonlinearities, such as saturation or accelerating consumption, can appear in the data which we do not consider in our framework or data compilation. For one of the data points b has a negative value which is not realistic. This is likely due to noise in the data or some unaccounted for physiological response of the particular species.

Experiments which can be used to estimate b often measure multiple consumption rates within a single experiment, for example substrate consumption and oxygen consumption. For our purposes here it is important to measure a resource which is directly proportional to the overall metabolic rate. In some cases it is essential to measure the limiting resource. For example in ref. [5] the carbon source is the limiting resource for growth and estimates of b using substrate consumption are an order of magnitude smaller than estimates obtained from oxygen consumption. This matters less in other studies where the two estimates can be nearly identical (e.g. ref. [6]).

For species where the conversion N between consumption rate and metabolic energy production is known, then it is possible to directly calculate E_m and B_m. For *E. coli* ref. [4] provides the number of moles of ATP produced per mole of oxygen consumed, denoted here as n. Combining values of n with considerations of ATP synthesis, the energy production conversion efficiency is given by $N = n\Delta G_{phos}$ where ΔG_{phos} $\left(\text{J} \cdot \text{mol ATP}^{-1}\right)$ is the phosphorylation potential of ATP. From ref. [7] for *E. coli* growing on glucose $\Delta G_{phos} = 4.65\times10^4$ $\left(\text{J} \cdot \text{mol ATP}^{-1}\right)$, from ref. [4] the aerobic energy conversion efficiency is $n = 4.31$ (mol ATP $\cdot$ mol O_2^{-1}), and the *E. coli* value for Y can be found in table S1. Given these values we calculate that $E_m = n\Delta G/Y = 3345$ (J $\cdot$ dry g^{-1}). This value

is comparable to values found previously for multicellular organisms which range from $E_m = 800$ to $E_m = 13000$ (J $\cdot$ dry g^{-1}) for embryos and juveniles of several species of birds, fish, and mammals [8] (also see supplement of ref. [9]). This suggests that the commonality in the unit energetics that we found in microbes may also extend to larger multicellular organisms.

Similarly, the maintenance cost for *E. coli* is given by $B_m = P\Delta G_{phos} n = .025$ (W $\cdot$ dry g cells $^{-1}$) for the experiment in ref. [4] which is carried out at 30° C (the temperature of the experiment is important given the temperature effects and normalizations discussed below).

Metabolic partitioning from individual cells and chemostat populations Using equation 11 from the main text it is possible to estimate $\bar{\gamma}$ given an estimate of μ for each species. We compiled estimates of μ_{max} for many of the species where we have already estimated b. We use μ_{max} to calculate $\bar{\gamma}$ because this represents a limiting value and also compares well to the single cell growth trajectories where the conditions are such that these individuals are often growing near their maximum rate. The data presented in figure 3B of the main text are the result of pairing b with measurements of μ_{max} and cell size.

Temperature normalization Following refs. [10, 11, 12] temperature has been shown to affect the total metabolic rate of an organism according to

$$B\left(T\right) = B\left(T_0\right) e^{E(T-T_0)/kTT_0} \tag{S6}$$

where it is assumed that this temperature dependence is carried by the normalization constant as

$$B_0\left(T\right) = B_0\left(T_0\right) e^{E(T-T_0)/kTT_0}, \tag{S7}$$

where E is an average activation energy for biochemical reactions, k is the Boltzmann constant, T is the operating temperature of an organism, and T_0 is a standard temperature of interest [10, 11, 12]. This has implications for several of the parameters that we use in our model which can be normalized to a common reference temperature. Following equation 3 of the main text, $Q\bar{m}N$ and $B_m = PN$ will each have the same temperature dependence as B, while $\bar{E_M} = N/Y$ will be independent of temperature consistent with previous assumptions [11]. These two relationships along with equation S7 demonstrate that the parameter $b = B_m/E_m$ from our model will depend on temperature while $\rho = \frac{B_m}{B_0} m^{1-\alpha}$ and $\gamma = 1 - \rho$ will not:

$$\begin{aligned} b\left(T\right) &= b\left(T_0\right) e^{E(T-T_0)/kTT_0} && \text{(S8)} \\ \rho\left(T\right) &= \rho\left(T_0\right) && \text{(S9)} \\ \gamma\left(T\right) &= \gamma\left(T_0\right). && \text{(S10)} \end{aligned}$$

For those data where the operating temperature T is reported we use these normalizations. In this paper we used $E = .6$ eV which has been shown to be the average value across a diverse set of organisms [10].

Derivation of the growth trajectory Typically the partitioning of equation 4 of the main text is rewritten as

$$\frac{dm}{dt} = am^{\alpha} - bm \tag{S11}$$

with $a = B_0/E_m$ ($\mathrm{g}^{1-\alpha}\ \mathrm{s}^{-1}$) and $b = B_m/E_m$ [13, 8]. The mass trajectory for a free value of α can then be solved as

$$m\left(t\right) = \left[1 - \left(1 - \frac{b}{a}m_0^{1-\alpha}\right)e^{-b(1-\alpha)t}\right]^{1/(1-\alpha)} \left(\frac{a}{b}\right)^{1/(1-\alpha)}. \tag{S12}$$

Recognizing that $\frac{b}{a} = \frac{B_m}{B_0}$ it follows that $\gamma_0 = 1 - \frac{b}{a}m_0^{1-\alpha}$ and we can rewrite this equation as

$$m\left(t\right) = \left[1 - \gamma_0 e^{-b(1-\alpha)t}\right]^{1/(1-\alpha)} \left(\frac{1}{1-\gamma_0}\right)^{1/(1-\alpha)} m_0 \tag{S13}$$

which is the form from the main text. This form is appealing because γ_0 is a nondimensional number bounded between zero and one, and the initial mass now appears as a simple factor.

Both systems of parameters are useful in different contexts and each makes certain interpretations of data more conceptually explicit (e.g. metabolic partitioning vs. unit costs).

Normalized growth trajectories Normalizing the lifespan, or rate of growth, reveals the general shifts in the metabolic partitioning between major taxonomic groups. Choosing the dimensionless time variable $\tau = b\left(1-\alpha\right)t - \ln\left(\gamma_0\right)$ Eq. S13 becomes $\gamma = e^{-\tau}$. The dimensionless temporal parameter τ accounts for differences in the overall metabolic and bioenergetic rates. This relationship is plotted in Fig. S2 along with each of the 6170 datapoints from the individual growth trajectories. All of the data lie tightly along the predicted curve reflecting an underlying commonality in the form of growth, and the goodness of fit of the model simultaneously across diverse species. On this curve taxa are separated based on differences in the relative metabolic power devoted to growth, γ. There is a constant decrease in γ as we move to longer normalized timescales which also corresponds to moving across the three evolutionary life-history transitions. This view highlights that prokaryotes and small unicellular eukaryotes live over relatively short normalized timescales and use almost all of their metabolism for growth; they truly "live fast and divide young" (Fig. S2).

In previous work similar normalizations have been used where the plot in ref. [13] can be interpreted as the fraction of metabolism devoted to maintenance (rather than growth

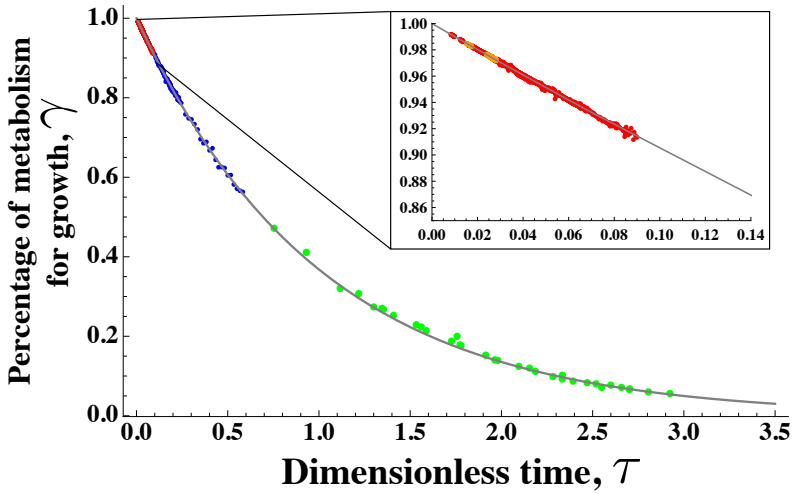

Figure S2: The universal metabolic partitioning curve for all of the individuals analyzed in this paper. Colors denote the three evolutionary life-history groups: prokaryotes (red), eukaryotes (blue), and small metazoans (green). The insert shows the two prokaryotic species with *E. coli* in red and *B. subtilis* in orange. The points in this plot are from 45 individual growth trajectories. Not all of the 6170 datapoints are individually distinguishable because of the tight clustering within this transformation.

as in Fig. S2) for a fixed value of $\alpha = 3/4$. Our free-α version accounts for differences in growth trajectories between individuals related to the overall metabolic scaling of an organism in addition to variation of the the unit bioenergetic costs.

Population Growth Rate In the main text we discussed the population growth rate, μ, of an organism which is based on our derivation of the generation time, G, along with the fecundity, f, and percentage of the population to reach the age of reproduction, L. In most of the single organism studies f and L are not measured in addition to the growth trajectory. In order to deal with this issue, along with the differing reproductive strategies across taxa, we introduce a "mass fecundity" where we consider the total mass production over the life cycle of an organism. That is, we define population growth rate by

$$\mu = \ln(\epsilon)/G \tag{S14}$$

where ϵ quantifies the factor change in body mass over a life-cycle, $M_d = \epsilon m_0$. These are the values reported in Fig. 3 of the main text.

Fitting the interspecific relationships for the population growth rate and the fraction of metabolism devoted to growth In the main text we present an interspecific fit for the dependence of population growth rate on body mass and from this we

are able to predict the fraction of metabolism devoted to growth for both prokaryotes and eukaryotes. It is useful to explicitly give the mass dependence of generation time which determines μ. Using equation S12 we can rewrite equation 9 from the main text as

$$G = \frac{1}{b\,(1-\alpha)} \ln \left[\frac{1 - \frac{b}{a} m_0^{1-\alpha}}{1 - \frac{b}{a} \left(\epsilon m_0\right)^{1-\alpha}} \right]. \tag{S15}$$

This form has the appealing features that the mass dependence is explicit and that the parameter a is based on unit costs and thus should be constant across organisms of different size similar to b and in contrast to γ_0 which depends on the initial mass of a cell. Using versions of the equations which depend on the parameter a is best suited for interspecific fits.

In fitting the interspecific data for prokaryotes and eukaryotes we fixed the value of b to the average for each group using our compilation (Fig. S1). We then find the best fit values of a and α for the interspecific data using a reduced major axis regression. The results for the best fit values of α are given in the main text.

We were unable to fit the interspecific data for the metazoans because it is unclear how features such as fecundity or ϵ, the ratio of reproductive mass to initial mass, change with body size. As discussed in the main text these alterations may be critical for allowing metazoans to grow larger while avoiding the limit where the fraction of energy devoted to biosynthesis goes to zero, as is the case for unicellular eukaryotes.

Similar to the generation time, the fraction of metabolism devoted to growth can be written in terms of the parameter a and cell mass using equation 7 (or 6 and 8) of the maintext:

$$\gamma = 1 - \frac{B_m}{B_0} m^{1-\alpha} = 1 - \frac{b}{a} m^{1-\alpha}. \tag{S16}$$

Using the taxonomic average value of b and the best fit values of a and α from the interspecific fit of population growth rate from above we are able to predict γ as a function of body size for prokaryotes and eukaryotes and these are the curves drawn in Fig. 3B of the main text.

As described above we cannot fit the interspecific data of growth rate for the metazoans using our framework for G and μ. In order to predict the interspecific relationship of $\bar{\gamma}$ we instead fit a power law to growth rate [16] and use equation 11 from the main text where we use the eukaryotic average for $\bar{b}$.

The growth of buds within the yeast complex Our hypothesis for the yeast complex is that when a new bud forms nearly all of the growth energy from the entire complex is devoted to that bud. This is to say that a bud grows with the metabolic energy of a much larger organism than its own size. In order to test this hypothesis we first fit our growth model for $m\,(t)$ to the entire complex and we then use those fit parameters to describe the growth trajectory of each bud in agreement with data. Fitting $m\,(t)$ to any

region of total complex will give a prediction of the mass at any subsequent time and from this the total growth rate of the entire complex at any given time is given by

$$\frac{dm}{dt} = am_{tot}(t)^{\alpha} - bm_{tot}(t) \tag{S17}$$

where it should be noted that $a = \frac{b}{\rho} m_0^{1-\alpha}$ (see equation S11), and the m_0 for the entire complex should be used. If all growth energy is devoted to the bud then the growth dynamics of the bud are described by

$$\begin{cases} \frac{dm_{bud}}{dt} = am_{tot}(t)^{\alpha} - bm_{tot}(t) \\ m_{tot}(t) = m_{tot}(t_b) + m_{bud} \\ m_{bud}(t_b) = m_0^{bud} \end{cases} \tag{S18}$$

or

$$\begin{cases} m_{bud}(t+\Delta t) = m_{bud}(t) + \Delta t\left[am_{tot}(t)^{\alpha} - bm_{tot}(t)\right] \\ m_{tot} = m_{tot}(t_b) + m_{bud} \\ m_{bud}(t_b) = m_0^{bud} \end{cases} \tag{S19}$$

where t_b is the time when a bud starts growing and m_0^{bud} is its initial size. The bud curves in figure 1D are the result of numerically integrating these dynamics for each bud. Thus each bud trajectory is not a fit but a prediction based on the growth dynamics of the entire complex. The fact that this agrees so well with the data for each bud supports the hypothesis that all growth energy is being devoted to a newly formed bud.

The reproductive strategy of diatoms Another example of an altered reproductive strategy is that used by some diatoms (including some of those discussed in [1]), which interrupt single cell growth with long resting phases [1]. Such cell types could not be analyzed with our framework, which only considers continuous growth. During a resting phase our model cannot interpret the energetics of the cell because there are no changes in size even though biosynthesis may be continuing. The two diatom species that we did examine were considered to grow continuously by ref. [1], yet we find here that an asymptotic mass just before division could signal a resting phase. Thus the low value of alpha found for these species could be the result of a different reproductive strategy (resting) rather than a metabolic constraint. Supporting this hypothesis, a terminal plateau has been previously observed in plant cells, where following nuclear division and separation of internal components by the cellular membrane the cell continues to build the cell wall for final cleavage [2]. This could lead to the apparent asymptote where biosynthesis is occurring but not being reflected by changes to the overall size of the cell. This is similar to the daughter buds of the yeast complex which approach an asymptote related to the dynamics of the entire complex rather than the value of the metabolic exponent α.

However, it should be noted that the low value of alpha could instead be due to the decrease in the ability for these organisms to harvest light resources with increasing cell

size based on the packaging of photosynthetic pigments [14]. Similarly, the metabolic scaling exponent has been shown to significantly decrease in light-limited growth conditions for phytoplankton [15]. There is not enough information yet to decipher if either of these effects, resting phases or changes in photosynthetic capacity, is leading to the low value of α.

Fitting routine for the growth trajectory We considered a least squares analogy for each individual growth trajectory where we minimize the sum

$$\sum_i \left[m_i - m\left(t_i, \gamma_0, b, \alpha\right)\right]^2 \tag{S20}$$

where m_i is the measured mass at measured time t_i, and $m\left(t_i, \gamma_0, b, \alpha\right)$ is given by equation 8 of the main text.

For the fits presented in the main text we use three free parameters (α, b, and γ_0). It should be noted that the statistical confidence in each best fit parameter is greatly increased by reducing the number of parameters fit. Below we discuss reduced parameter fits which yield slightly different results.

The optimization of equation S20 involves many local minima and for this reason we employed a heuristic algorithm. We used the Nelder-Mead simplex algorithm as implemented by the "NelderMead" method from the numerical minimization function "NMinimize" of the Mathematica software. All of the options were set to the Mathematica defaults. We seeded the algorithm with 48 distinct random initial values and allowed the algorithm to minimize the function thus finding a local minimum. We then compared each of these local minima and selected as the best fit the minimum with the lowest sum of square residuals. In many cases the various random seeds yielded very similar sets of parameters with only slightly different sums.

The method requires bounds to be set for each of the three parameters to be fit (α, b, γ_0). By definition gamma is required to be between 0 and 1. For α we know the experimental range across taxa from [16] and we take the bounds to be generously larger than this for the search. For b we allowed the search to include values that were two orders of magnitude larger and smaller than an initial guess. The initial guess was based on chemostat experiments where we were able to find previously published chemostat experiments under similar growth conditions as the single cell experiments for *E. coli* [4], *B. subtilis* [17], *C. albicans* [5], and *T. weissflogii* [18]. We were unable to locate chemostat experiments for *L. borealis* where we instead used *T. weissglogii* [18] as a guess; similarly for the two copepods we used *Brachionus calyciflorus* [19]. The Nelder-Mead algorithm also requires that we choose a range of parameter values in which to choose the initial points of the simplex. For each parameter this range was the same as these bounds except for b. We found that if b is sampled over too large a range then the fits are not tightly constrained (see reduced parameter fit below). The initial guesses should represent the relatively small variation in b that we observed in the chemostat experiments between

species, taxa, and various growth conditions (Tables S1-S2). For a species such as *E. coli* b was observed to vary by about a factor of 2. Thus for those species where we have a chemostat estimate for b our initial simplex sampling includes points that are 1.5 times larger or smaller than the initial guess, leading to a sampling that covers a factor of roughly 2. When we do not have a species estimate (diatoms and copepods) we allow more flexibility in b and sample initial points over an order of magnitude centered on the initial guess. As the minimization runs the values of b are still allowed to range between the bounds described above (over 4 orders of magnitude).

We used a fixed initial mass for each fit. For data where mass is given at $t = 0$ we take this to be m_0, for instances where the initial time point is close to zero relative to the length of the time series we use a linear fit to the first third of the data to estimate m_0. For cases where the initial timepoint is not close to zero (*Calanus pacificus*) we used an exponential fit to the first third of the data to estimate m_0.

Reduced parameter fits. Reducing the number of parameters in the model greatly increases the statistical confidence of the best fit value for each parameter. Yet this comes with a decision about which parameter to fix. In previous studies α is taken to be fixed [13, 8, 11, 9], but ref. [16] illustrates that this exponent varies between taxa and it is thus reasonable to consider that it might also vary between species. The parameter b can be estimated from population studies which allows us to examine the value for a single species independent of the growth trajectory fits. This is not commonly possible for α at present.

We first tested the effect of imposing a fixed value of α for each of the growth trajectory fits. For each fit we choose the appropriate value of α based on taxonomy ($\alpha = 1.96$ for prokaryotes, $\alpha = 1.06$ for eukaryotes, and $\alpha = .79$ for metazoans [16]). We found that these fixed-α fits can cause the best fit value of b to disagree with the population estimates by an order of magnitude or more. For example in *E. coli* using the free value of α yields an average b of $5.50 \pm 2.31 \times 10^{-6}$ which compares well with chemostat estimates of $b = 3.35 \times 10^{-6}$ for cells growing under very similar conditions; while using the fixed interspecific value of $\alpha = 1.96$ gives $b = 1.47 \pm 3.22 \times 10^{-5}$ which does not agree as closely with chemostat estimates and has greater variance in the best fit values. These fits also have lower R^2 values compared to the free α and fixed-b (discussed below) fits.

Given that for most species we can estimate b from measurements of the same species in a chemostat it perhaps makes more sense to treat these values as constant in a reduced parameter fit. Here we explicitly fix b to chemostat estimates and fit the growth trajectories using only α and γ_0. The resulting best-fit α and γ_0 values are given in Fig. S3 where it can be seen that these fits are similar to those found using a free value of b, but we find that the statistical confidence in each parameter is much higher. We fixed the value of b to the population estimate for the same species except for *L. borealis* where we instead used the value for *T. weissglogii* [18] and for the two copepods we used *Brachionus calyciflorus* [19].

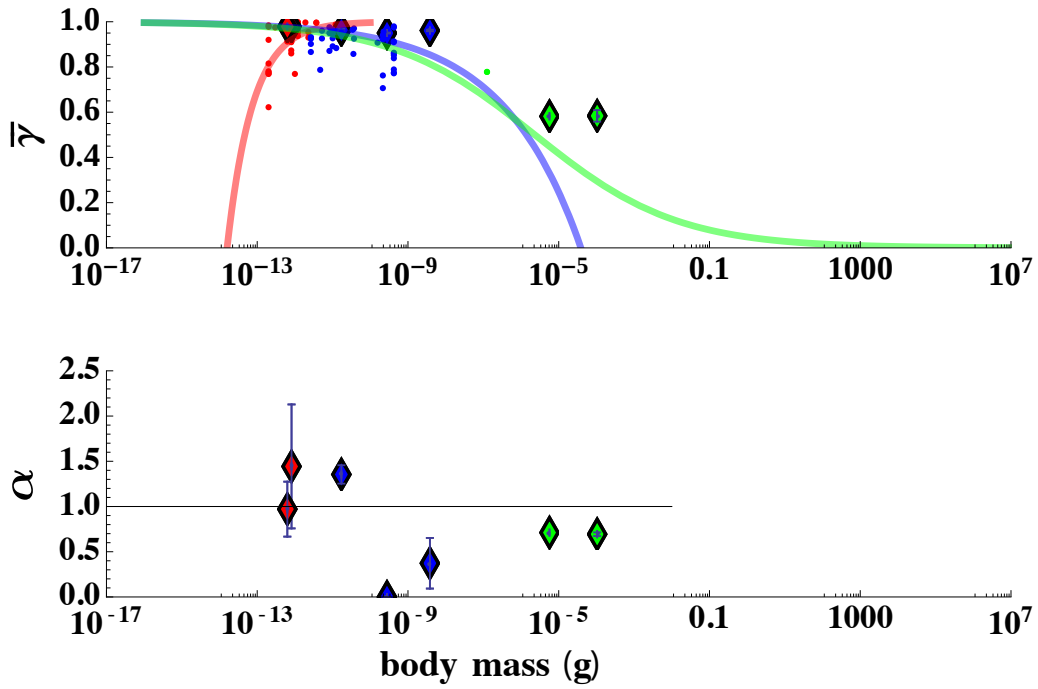

Figure S3: Results from reduced parameter fits to the individual growth trajectories. The best fit values for the metabolic scaling exponent, α, and the average fraction of metabolism devoted to growth, $\bar{\gamma}$, are shown given b fixed to chemostat estimates for each species. All other lines and data are the same as Fig. 3 of the main text.

Conversions between measurements of size In this study we considered all mass data in terms of dry mass. However, the original sources presented their data in terms of many different units for measuring size: wet, dry and carbon weights, cell volume, and bouyant mass. Here we present our methodology for converting between these quantities. These conversions are summarized in table S3.

We convert between volume and dry weight, m_{dry}, using the relationship

$$m_{dry} = \beta_2 V^{\eta_1} \tag{S21}$$

where empirically, in the units of the original paper, $\eta_1 = .86$ and $\beta_2 = 435$ (dry fg $\mu\text{m}^{-\eta_1}$) for *E. coli* [20] and $\eta_1 = .91$ and $\beta_2 = 162$ (dry fg $\mu\text{m}^{-\eta_1}$) for a variety of bacteria [21].

The carbon content of a cell C has been shown to follow

$$C = \beta_3 V^{\eta_2} \tag{S22}$$

[22] which given the relationship for dry weight implies that

$$m_{dry} = \beta_2 \left(\frac{C}{\beta_3}\right)^{\eta_1/\eta_2}. \tag{S23}$$

Table S3: Allometric conversions

Property	**Relationship**	**Ref.**
Dry, m_{dry}, and wet weight m_{wet}	$m_{dry} = \beta_1 m_{wet} \quad \beta_1 \approx .22$	[23]
Volume, V_c, and dry weight m_{dry}	$m_{dry} = \beta_2 V_c^{\eta_1}$	
E. coli	$\eta_1 = .86 \quad \beta_2 = 435$ (dry fg μm$^{-\eta_1}$)	[20]
Bacteria	$\eta_1 = .91 \quad \beta_2 = 162$ (dry fg μm$^{-\eta_1}$)	[21]
Carbon content C and cell volume, V_c, and dry weight m_{dry}	$C = \beta_3 V^{\eta_2}$	
	$\eta_2 = .89 \quad \beta_3 = 224$ (dry fg C μm$^{-\eta_2}$)	[22]
Buoyant mass m_b and dry weight m_{dry}	$m_{dry} = \beta_2 \left(\frac{C}{\beta_3}\right)^{\eta_1/\eta_2}$	derived from refs. [22, 20, 21]
Carbon content C and dry weight m_{dry}	$m_{dry} = \frac{\beta_1 m_b}{1-\frac{\delta_f}{\delta_c}} \quad \delta_c = 1.1 \times 10^6$ (g m^{-3})	[23]

Empirically, $\eta_2 = .89$ and $\beta_3 = 224$ (dry fg C μm$^{-\eta_2}$) [22] and thus $m_{dry} \approx 2.33C^{.97}$ (fg).

We assume that dry weights scale isometrically with wet weight, m_{wet}, such that

$$m_{dry} = \beta_1 m_{wet}. \tag{S24}$$

It is observed that an appropriate average for several species including *E. coli* and *B. subtilis* is $\beta_1 = .22$ [23] which agrees with other estimates ($\beta_1 \approx .3$) for *E. coli* and a mammalian cell [24, 25, 26].

Bouyant mass m_b is related to wet weight as

$$m_b = m_{wet}\left(1 - \frac{\delta_f}{\delta_c}\right) \tag{S25}$$

where δ_f is the density of the fluid in which the cell is suspended, and δ_c is the density of the cell. The dry mass is then given by

$$m_{dry} = \frac{\beta_1 m_b}{1 - \frac{\delta_f}{\delta_c}}. \tag{S26}$$

We use a cell density of $\delta_c = 1.1 \times 10^6$ (g m^{-3}) which is representative of several bacterial species [23].

Data compilation for single-cell growth trajectories For the single cell analysis we obtained growth trajectories from several previously published sources [27, 28, 1, 29, 30, 31]. We were able to obtain the original data and numerical values from the authors for *E. coli* from refs. [27, 28] and *B. subtilis* from ref. [30]. For the two species of diatoms (*Thalassiosira weissflogii* and *Lauderia borealis*) given in ref. [1], *C. albicans* from ref. [29], and the two species of copepods (*Calanus pacificus*, and *Pseudocalanus sp.*) from ref. [31] we obtained values by digitizing the growth trajectory figures from each paper using the software GraphClick. Below is a more detailed discussion of the growth data from each study.

Calculating mass for *E. coli* For the analysis of a single *E. coli* cell we used the data presented in ref. [27, 28]. In order to calculate cell volume we employed the shape model from ref. [28] where *E. coli* growth is divided into two periods: first, the cell is treated as cylinder with two hemispherical caps, and new biomass results in the simple elongation of the cylindrical portion of the cell; second, the middle of the cell undergoes a constriction and the relationship between biomass production and volume becomes more complicated, where the constricted region can be treated as two intersecting hemispheres of equal size to the caps [28]. The cylinder and the two caps are taken to have the same radius. We obtained data from the authors for the cell length and relative "waist width" time-series presented in ref. [27, 28] along with the noted onset of constriction. From this we extracted the time series of cell volume given the reported average diameter of $d = .933$ (μm) [27, 28]. We convert this to mass using the allometric relationship in table S3.

Calculating mass for budding yeast For the analysis of a budding yeast complex (*Candida albicans*) we used the data from ref. [29]. These data relied on optical methods for tracking cell size. The yeast data is reported in volume units and we convert to mass using the scaling law described in table S3.

Calculating mass for the diatoms Data for single diatoms came from ref. [1] where changes in relative length were measured optically. We first convert to volume using a cylindrical cell shape model along with the constant diameter and initial length of the cell given in ref. [1]. We assume that each cell has the same initial length. We analyzed the two species *T. weissflogii* and *L. borealis*. Our theory concerns the time required to produce a unit of mass, and thus we did not analyze the three diatom species (*S. turris*, *B. aurita*, and *Coscinodiscus sp.*) presented in ref. [1] because they have long periods of dormancy which is not addressed in our model.

Calculating mass for *B. subtilis* In Ref. [30] the buoyant mass of single *B. subtilis* cells are measured over the course of life cycle with very high temporal resolution. The dry mass of the cell can be calculated using equation S26 where we approximate the fluid density with that of water.

Copepod data mass Two species of copepods are analyzed in ref. [31], *C. pacificus* and *Pseudocalanus sp.*. The data represent the population average growth trajectory for the mass of a single individual. This is distinct from tracking one individual through a growth cycle, but represents the tracking many individuals and then averaging. Each of the curves represents this average growth trajectory in different nutrient (prey) conditions. This study varied the type of prey, prey size, and prey concentrations. We picked the fastest growing curve from each set of prey conditions. The original study also varied the growing temperature but we considered only those curves grown at a temperature most similar to the unicellular studies (15° C).

Parameter values from the individual growth trajectories Table S4 provides the best fit parameter values for each of the individual growth trajectories. These are results from allowing α, b, and γ_0 to be free parameters as described earlier in the supplement.

Definition of symbols Table S5 provides definitions for each symbol or variable used in our framework.

Species	Type	m_0	γ_0	$\hat{\gamma}$	b	α	Number of cells	Refs.
		Initial mass (dry g)	Initial percentage of metabolism for growth	Average percentage of metabolism for growth	Metabolic cost ratio rate (B_m/E_m) (s^{-1}) normalized to 20° C	Metabolic scaling exponent		
B. subtilis	Prokaryote	$4.5\pm0.41\times10^{-13}$	0.978±0.006	0.977±0.005	$3.08\pm0.76\times10^{-6}$	0.97±0.31	3	[30]
E. coli	Prokaryote	$6.21\pm0.56\times10^{-13}$	0.963±0.018	0.966±0.014	$5.5\pm2.31\times10^{-6}$	1.43±0.67	30	[27, 28]
C. albicans	Unicellular eukaryote	$8.7\pm1.\times10^{-12}$	0.947±0.001	0.955±0.004	$9.49\pm0.55\times10^{-7}$	1.35±0.1	2	[29]
T. weissflogii	Unicellular eukaryote	$1.91\pm0.02\times10^{-10}$ †	0.912±0.016	0.873±0.02	$1.29\pm0.24\times10^{-6}$	0.01±0.01	3	[1]
L. borealis	Unicellular eukaryote	$2.54\pm0.05\times10^{-9}$ †	0.82±0.048	0.768±0.097	$3.62\pm1.89\times10^{-6}$	0.47±0.23	3	[1]
Pseudocalanus sp.	Metazoan	$1.8\pm0.\times10^{-6}$	0.471±0.	0.366±0.	$5.95\pm0.\times10^{-6}$	0.82±0.	1	[31]
C. pacificus	Metazoan	$4.95\pm0.98\times10^{-6}$	0.265±0.022	0.139±0.008	$2.42\pm0.01\times10^{-5}$	0.93±0.	4§	[31]
Multi-species Population Compilation:								
	Prokaryote average	——	No data	mass dependent	$5.79\pm9.99\times10^{-6}$	No data	138	see SI
	Eukaryote average	——	No data	mass dependent	$3.39\pm3.17\times10^{-6}$	No data	52	see SI

† Data presented in ref. [1] are given in units of relative mass, these are based on the reported lower bound on size

§ This average is conducted across individuals living in different nutrient conditions (see supplement).

Table S4: The energetic constants obtained by fitting our model to single cell growth trajectories.

Symbol	Name	Units
a	Ratio of the metabolic normalization constant (B_0) to the unit biosynthetic cost (E_m)	$g^{1-\alpha}\ s^{-1}$
α	Metabolic scaling exponent	Dimensionless
b	Ratio of the maintenance metabolic rate (B_m) to the unit biosynthetic cost (E_m)	s^{-1}
B	Total metabolic rate	W
B_0	Size-normalized metabolic constant	$(W\ g^{-\alpha})$
B_m	Metabolic expenditure to support a unit of mass	$(W\ g^{-1})$
ϵ	Ratio of division mass to initial mass	Dimensionless
E_m	Energy to synthesize a unit of mass	$(J\ g^{-1})$
γ	Percentage of metabolism devoted to growth	Dimensionless
γ_0	Percentage of metabolism devoted to growth at the initial size	Dimensionless
$\bar{\gamma}$	Percentage of metabolism devoted to growth averaged over a population in a chemostat	Dimensionless
$\hat{\gamma}$	Percentage of metabolism devoted to growth averaged over the life-cycle of an individual	Dimensionless
G	Generation time	s
ΔG	Phosphorylation potential	$(J \cdot ATP^{-1})$
m	Mass of the cell at any given time	g
m_0	Initial mass of the organism	g
m_d	Division mass of the organism	g
μ	Specific growth rate	s^{-1}
N	Conversion constant for resource use to metabolic power production	(J mol resource $^{-1}$)
n	ATP yield from oxygen	Mol ATP $\cdot$ Mol $O_2{}^{-1}$
P	Maintenance requirement	(mol resource $\cdot$ s^{-1} $\cdot$ g cells $^{-1}$)
Q	Specific consumption rate	(mol resource $\cdot$ s^{-1} $\cdot$ g cells $^{-1}$)
ρ	Percentage of metabolism devoted to maintenance	Dimensionless
Y	Yield coefficient	(g cells $\cdot$ mol resource $^{-1}$)

Table S5: Table of variables.

Individual growth curves Here we present fits for each individual cell that we examined. In each plot the dots represent the compiled data for cell mass against time, and the red line is the best fit of Eq. 8 (of the main text) to the growth trajectory.

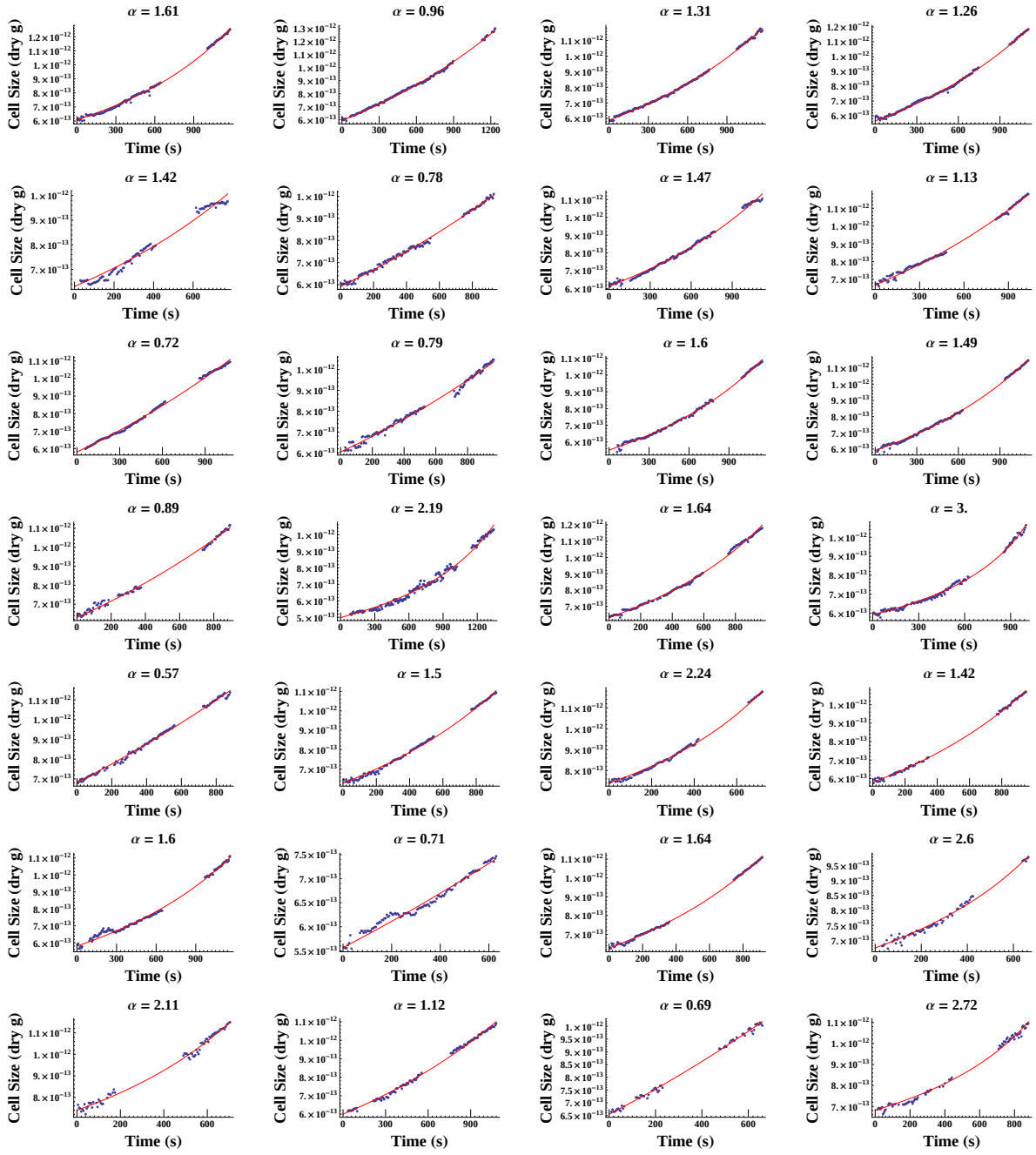

Figure S4: ***E. coli*** Data from [27, 28].

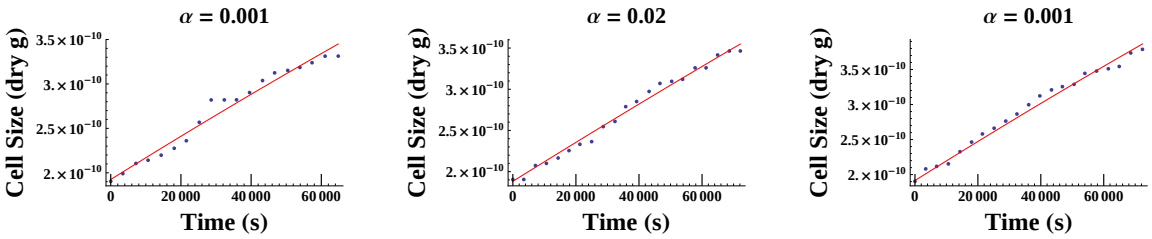

Figure S5: ***T. weissflogii*** Data from [1].

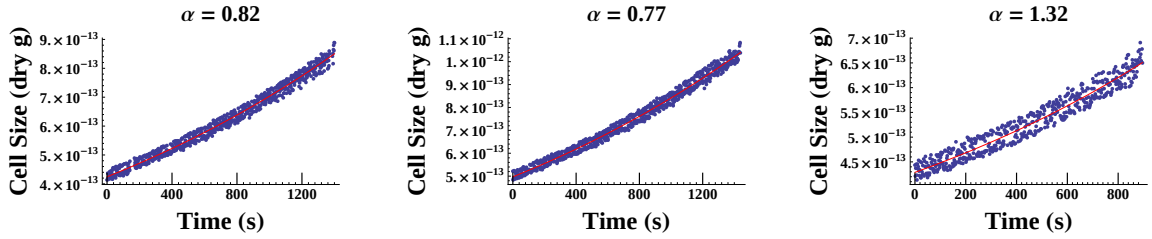

Figure S6: ***B. subtilis*** Data from [30].

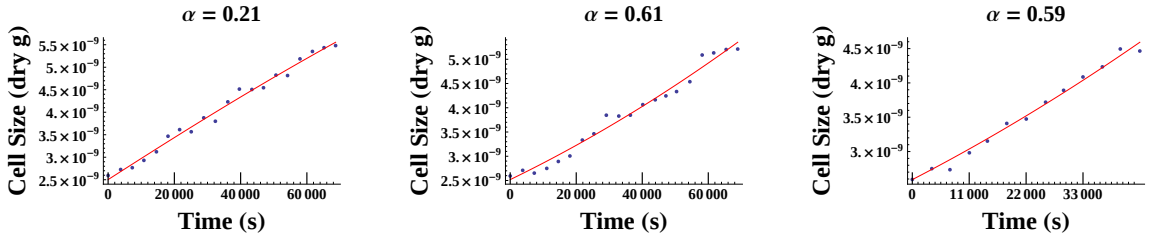

Figure S7: ***L. borealis*** Data from [1].

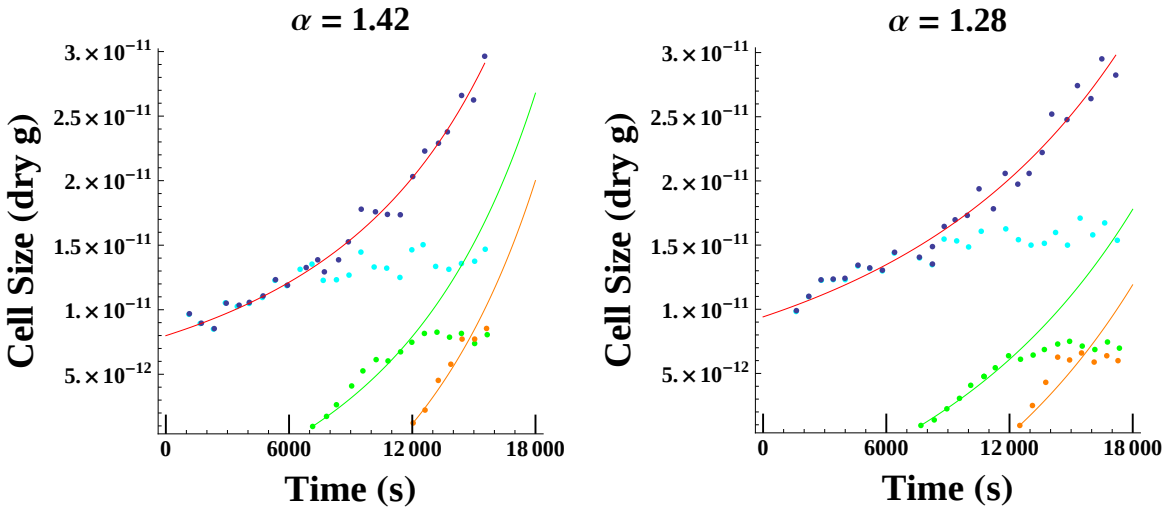

Figure S8: **Entire *C. albicans* complex.** This mirrors figure 1D of the main text where the red curve is the fitted growth trajectory for the entire complex of budding yeast (dark blue points) which initially starts from a single mother bud (cyan points). The significance of the mother bud is that its growth slows with the formation of the first (green points) and second (orange points) daughter buds whose predicted trajectories (see Eq. S18) are also shown using the same color scheme. The fitted exponent is for the entire complex. Data is from ref. [29].

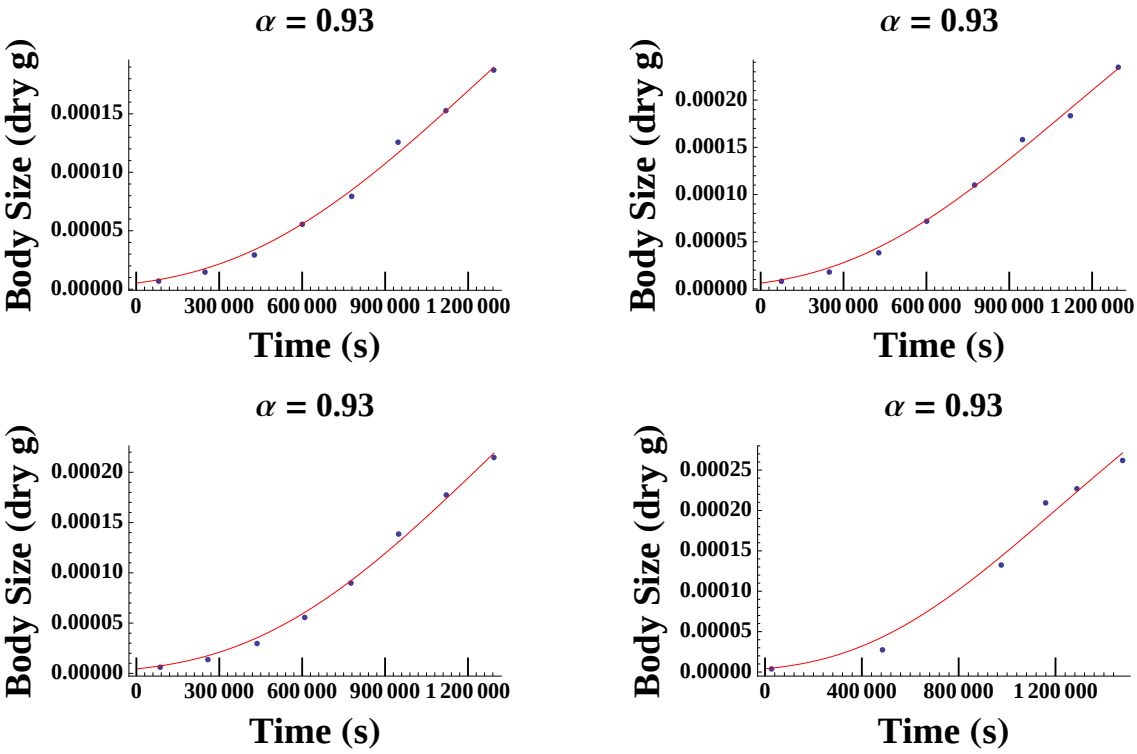

Figure S9: ***C. pacificus*** Data from [31].

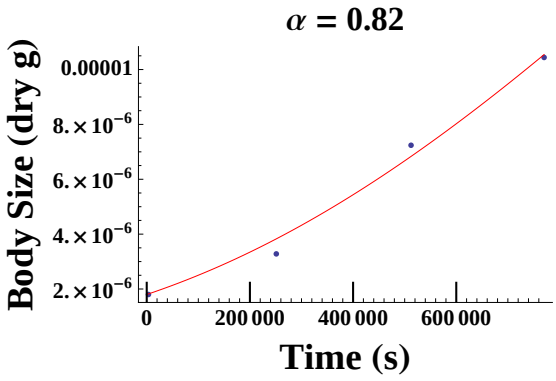

Figure S10: ***Pseudocalanus sp.*** Data from [31].

Supporting Information References

[1] Olson R, Watras C, Chisholm S (1986) Patterns of individual cell growth in marine centric diatoms. *Microbiology* 132:1197.

[2] Mitchison J (1971) *The biology of the cell cycle* (Cambridge University Press).

[3] Pirt S (1965) The maintenance energy of bacteria in growing cultures. *Proceedings of the Royal Society of London. Series B, Biological Sciences* 163:224–231.

[4] Farmer I, Jones C (1976) The energetics of Escherichia coli during aerobic growth in continuous culture. *European Journal of Biochemistry* 67:115–122.

[5] Shepherd M, Sullivan P (1976) The production and growth characteristics of yeast and mycelial forms of Candida albicans in continuous culture. *Microbiology* 93:361–370.

[6] Schulze K, Lipe R (1964) Relationship between substrate concentration, growth rate, and respiration rate of escherichia coli in continuous culture. *Archives of Microbiology* 48:1–20.

[7] Tran Q, Unden G (1998) Changes in the proton potential and the cellular energetics of Escherichia coli during growth by aerobic and anaerobic respiration or by fermentation. *European Journal of Biochemistry* 251:538–543.

[8] Moses M, et al. (2008) Revisiting a model of ontogenetic growth: estimating model parameters from theory and data. *The American Naturalist* 171:632–645.

[9] Hou C, et al. (2008) Energy uptake and allocation during ontogeny. *Science* 322:736.

[10] Gillooly J, Brown J, West G, Savage V, Charnov E (2001) Effects of size and temperature on metabolic rate. *Science* 293:2248.

[11] Gillooly J, Charnov E, West G, Savage V, Brown J (2002) Effects of size and temperature on developmental time. *Nature* 417:70–73.

[12] Savage V, Gillooly J, Brown J, West G, Charnov E (2004) Effects of body size and temperature on population growth. *The American Naturalist* 163:429–441.

[13] West G, Brown J, Enquist B (2001) A general model for ontogenetic growth. *Nature* 413:628–631.

[14] Niklas, K. (1994) *Plant allometry: the scaling of form and process.* (University of Chicago Press).

[15] Finkel, ZV, Irwin, AJ, Schofield, O. (2004) Resource limitation alters the 3/4 size scaling of metabolic rates in phytoplankton. *Marine Ecology Progress Series* 273:269–279.

[16] DeLong J, Okie J, Moses M, Sibly R, Brown J (2010) Shifts in metabolic scaling, production, and efficiency across major evolutionary transitions of life. *Proceedings of the National Academy of Sciences* 107:12941–12945.

[17] Sauer U, et al. (1996) Physiology and metabolic fluxes of wild-type and riboflavin-producing Bacillus subtilis. *Applied and environmental microbiology* 62:3687–3696.

[18] Falkowski P, Dubinsky Z, Wyman K (1985) Growth-irradiance relationships in phytoplankton. *Limnology and oceanography* 30:311–321.

[19] Boraas M (1983) Population dynamics of food-limited rotifers in two-stage chemostat culture. *Limnology and Oceanography* 28:546–563.

[20] Loferer-Krossbacher M, Klima J, Psenner R (1998) Determination of bacterial cell dry mass by transmission electron microscopy and densitometric image analysis. *Applied and Environmental Microbiology* 64:688.

[21] Norland S, Heldal M, Tumyr O (1987) On the relation between dry matter and volume of bacteria. *Microbial Ecology* 13:95–101.

[22] Løvdal T, Skjoldal E, Heldal M, Norland S, Thingstad T (2008) Changes in morphology and elemental composition of Vibrio splendidus along a gradient from carbon-limited to phosphate-limited growth. *Microbial Ecology* 55:152–161.

[23] Bratbak G, Dundas I (1984) Bacterial dry matter content and biomass estimations. *Applied and Environmental Microbiology* 48:755.

[24] Cayley S, Lewis B, Guttman H, Record Jr M (1991) Characterization of the cytoplasm of Escherichia coli K-12 as a function of external osmolarity. Implications for protein-DNA interactions in vivo. *Journal of molecular biology* 222:281.

[25] Neidhardt F (1996) *Escherichia coli and Salmonella: Cellular and Molecular Biology. Vol. 1* (ASM Press).

[26] Bray D (2001) *Cell movements: from molecules to motility* (Routledge).

[27] Reshes G, Tsukanov R, Vanounou S, Fishov I, Feingold M (2009) Timing the start of division in E. coli: a single-cell study. *Biophysical Journal* 96:631–631.

[28] Reshes G, Vanounou S, Fishov I, Feingold M (2008) Timing the start of division in E. coli: a single-cell study. *Physical Biology* 5:046001.

[29] Herman M, Soll D (1984) A comparison of volume growth during bud and mycelium formation in Candida albicans: a single cell analysis. *Microbiology* 130:2219.

[30] Godin M, et al. (2010) Using buoyant mass to measure the growth of single cells. *Nature Methods* 7:387–390.

[31] Vidal J (1980) Physioecology of zooplankton. I. Effects of phytoplankton concentration, temperature, and body size on the growth rate of Calanus pacificus and Pseudocalanus sp. *Marine Biology* 56:111–134.

[32] Tännler S, Decasper S, Sauer U (2008) Maintenance metabolism and carbon fluxes in bacillus species. *Microbial cell factories* 7:19.